Research Article | Vol. 25, No. 13 | 26 Jun 2017 | OPTICS EXPRESS 15299
Optics EXPRESS

Performance analysis of a coherent free space optical communication system based on experiment

JINGTAI CAO,[1,2] XIAOHUI ZHAO,[1] WEI LIU,[1,3] AND HAIJUN GU[1,*]

[1]College of Communication Engineering, Jilin University, 5372 Nanhu Road, Changchun, Jilin 130012, China
[2]Changchun Institute of Optics, Fine Mechanics and Physics, Chinese Academy of Sciences, 3888, Nanhu Road, Changchun 130033, China
[3]College of Geoexploration Science and Technology, Jilin University, Changchun, Jilin 130026, China
[*]ghyciom@163.com

Abstract: Based on our previous study and designed experimental AO system with a 97-element continuous surface deformable mirror, we conduct the performance analysis of a coherent free space optical communication (FSOC) system for mixing efficiency (ME), bit error rate (BER) and outage probability under different Greenwood frequency and atmospheric coherent length. The results show that the influence of the atmospheric temporal characteristics on the performance is slightly stronger than that of the spatial characteristics when the receiving aperture and the number of sub-apertures are given. This analysis result provides a reference for the design of the coherent FSOC system.

OCIS codes: (060.0060) Fiber optics and optical communications; (010.1080) Active or adaptive optics; (010.1330) Atmospheric turbulence; (060.1660) Coherent communications.

References and links

1. X. Ma, J. Sun, Y. Zhi, Y. Zhou, W. Lu, P. Hou, Q. Xu, and L. Liu, "Performance analysis of pupil-matching optical differential receivers in space-to-ground laser communication," Appl. Opt. **53**(14), 3010–3018 (2014).
2. K. Yao, J. Wang, X. Liu, H. Li, M. Wang, B. Cui, and S. Yu, "Pyramid wavefront sensor using a sequential operation method," Appl. Opt. **54**(13), 3894–3901 (2015).
3. S. Wang, C. Rao, H. Xian, J. Zhang, J. Wang, and Z. Liu, "Laboratory demonstrations on a pyramid wavefront sensor without modulation for closed-loop adaptive optics system," Opt. Express **19**(9), 8135–8150 (2011).
4. J. Perez, S. Zvanovec, Z. Ghassemlooy, and W. O. Popoola, "Experimental characterization and mitigation of turbulence induced signal fades within an ad hoc FSO network," Opt. Express **22**(3), 3208–3218 (2014).
5. K. Yao, J. Wang, X. Liu, and W. Liu, "Closed-loop adaptive optics system with a single liquid crystal spatial light modulator," Opt. Express **22**(14), 17216–17226 (2014).
6. L. Chen, J. Wang, K. Yao, X. Liu, X. Lin, L. Wang, and M. Wang, "Experimental demonstration of sequential operation approach for three-sided pyramid wavefront sensor," IEEE Photonics J. **8**(4), 2701113 (2016).
7. W. Liu, W. Shi, K. Yao, J. Cao, P. Wu, and X. Chi, "Fiber Coupling efficiency analysis of free space optical communication systems with holographic modal wavefront sensor," Opt. Laser Technol. **60**, 116–123 (2014).
8. J. Cao, X. Zhao, Z. Li, W. Liu, and Y. Song, "Stochastic parallel gradient descent laser beam control algorithm for atmospheric compensation in free space optical communication," Optik (Stuttg.) **125**(20), 6142–6147 (2014).
9. W. Liu, W. Shi, J. Cao, Y. Lv, K. Yao, S. Wang, J. Wang, and X. Chi, "Bit error rate analysis with real-time pointing errors correction in free space optical communication systems," Optik (Stuttg.) **125**(1), 324–328 (2014).
10. A. Belmonte, A. Rodríguez, F. Dios, and A. Comerón, "Phase compensation considerations on coherent, free-space laser communication system," Proc. SPIE **6736**, A11 (2007).
11. A. Belmonte, "Influence of atmospheric phase compensation on optical heterodyne power measurements," Opt. Express **16**(9), 6756–6767 (2008).
12. M. Li and M. Cvijetic, "Coherent free space optics communications over the maritime atmosphere with use of adaptive optics for beam wavefront correction," Appl. Opt. **54**(6), 1453–1462 (2015).
13. J. Li, Z. Zhang, J. Gao, J. Sun, and W. Chen, "Bandwidth of adaptive optics system in atmospheric coherent laser communication," Opt. Commun. **339**, 254–260 (2016).
14. L. Zuo, Y. Ren, A. Dang, and H. Guo, "Performance of coherent BPSK systems using phase compensation and diversity techniques," in *Proceedings of IEEE Conference on Global Telecommunication* (IEEE, 2010), pp. 1–5.
15. L. Zuo, A. Dang, Y. Ren, and H. Guo, "Performance of phase compensated coherent free space optical communication through non-Kolmogorov turbulence," Opt. Commun. **28**, 41491–41495 (2011).

#294590 https://doi.org/10.1364/OE.25.015299
Journal © 2017 Received 26 Apr 2017; revised 14 Jun 2017; accepted 18 Jun 2017; published 22 Jun 2017

Optics EXPRESS

16. C. Liu, S. Chen, X. Li, and H. Xian, "Performance evaluation of adaptive optics for atmospheric coherent laser communications," Opt. Express **22**(13), 15554–15563 (2014).
17. C. Liu, M. Chen, S. Chen, and H. Xian, "Adaptive optics for the free-space coherent optical communication," Opt. Commun. **361**, 21–24 (2016).
18. H. Jian, D. Ke, L. Chao, Z. Peng, J. Dagang, and Y. Zhoushi, "Effectiveness of adaptive optics system in satellite-to-ground coherent optical communication," Opt. Express **22**(13), 16000–16007 (2014).
19. J. Huang, H. Mei, K. Deng, L. Kang, W. Zhu, and Z. Yao, "Signal to noise ratio of free space homodyne coherent optical communication after adaptive optics compensation," Opt. Commun. **356**, 574–577 (2015).
20. W. Liu, K. Yao, D. Huang, X. Lin, L. Wang, and Y. Lv, "Performance evaluation of coherent free space optical communications with a double-stage fast-steering-mirror adaptive optics system depending on the Greenwood frequency," Opt. Express **24**(12), 13288–13302 (2016).
21. R. Tyson, Principles of Adaptive Optics, 3rd ed. (CRC, 2010).
22. J. Huang, C. Liu, K. Deng, Z. Yao, H. Xian, and X. Li, "Probability of the residual wavefront variance of an adaptive optics system and its application," Opt. Express **24**(3), 2818–2829 (2016).
23. S. Gladysz, J. C. Christou, L. W. Bradford, and L. C. Roberts, "Temporal Variability and Statistics of the Strehl Ratio in Adaptive-Optics Images," Publ. Astron. Soc. Pac. **120**(872), 1132–1143 (2008).
24. J. Ma, K. Li, L. Tan, S. Yu, and Y. Cao, "Performance analysis of satellite-to-ground downlink coherent optical communications with spatial diversity over Gamma-Gamma atmospheric turbulence," Appl. Opt. **54**(25), 7575–7585 (2015).
25. M. Niu, J. Cheng, and J. F. Holzman, "Exact error rate analysis of equal gain and selection diversity for coherent free-space optical systems on strong turbulence channels," Opt. Express **18**(13), 13915–13926 (2010).

1. Introduction

Free space optical communication (FSOC) systems play a significant role in modern communication for its high communication speed, free license spectrum, and excellent security. They can be considered as an important technology for the supplement of both traditional wireless communication systems and fiber optics communication systems. Recently, coherent FSOC systems have attracted more attentions compared with the FSOC systems using intensity modulation direct detection, due to their higher sensitivity, longer relay distance, larger communication capacity, and better receiver selectivity [1–4]. Despite many advantages of the coherent FSOC systems, they are still vulnerable to the atmospheric turbulence, since wavefront and amplitude of laser carrier signal are distorted by this turbulence with time in free space, which will definitely increase system BER and outage probability, and decrease system mixing efficiency (ME). In other words, the performance of the coherent FSOC system becomes worse. Fortunately, the developments of adaptive optics (AO) can compensate this weakness for FSOC systems by successfully mitigating the turbulence-induced wavefront aberrations of the received laser carrier signal [5–9].

Generally the spatial characteristics of atmospheric turbulence or atmospheric coherent length have influence on the performance of the coherent FSOC system. In order to analyze this performance, majority of researchers use these characteristics to evaluate the atmospheric turbulence. In fact, the temporal characteristics of the atmospheric turbulence or the Greenwood frequency (GF) also exert impact on the FSOC system. And under certain conditions, the influence of the temporal characteristics is stronger than that of the spatial characteristics.

The study of the coherent FSOC with an AO unit had been under rapid progress. Many existing research works focused on the performance analysis of the coherent FSOC based on an AO unit with different spatial characteristics. Aniceto Belmonte analyzed the capacity of coherent FSOC links with atmospheric compensation techniques, and evaluated the influence of atmospheric phase compensation on optical heterodyne power measurements. The obtained results were the ratio of receiver aperture diameter to wavefront coherent diameter, the strength of scintillation index, and the number of Zernike modes compensated. The compensated phase of the heterodyne receivers offered potentiality to overcome the limitations imposed by partial correction of the turbulence induced wavefront phase aberrations. However, the wavefront amplitude fluctuations limited the compensation process so that the achievable heterodyne performance reduced [10,11]. According to maritime condition, Ming Li et al. established a coherent FSOC channel model. A comprehensive

Optics EXPRESS

performance comparison between maritime and terrestrial atmospheric links was also conducted. And the comparison results showed that BER of the coherent FSOC system can be significantly improved by AO unit [12]. Jiawei Li et al. performed the bit error rate (BER) performance analysis for a coherent FSOC system with binary phase shift keying (BPSK) modulation. For the temporal characteristics, the servo bandwidth was investigated using multiple different values [13]. Zuo et al. investigated the BER performance of coherent FSOC links in weak non-Kolmogorov turbulence and showed that BER decreased sharply when more Zernike modes were corrected by AO unit. In consideration of the influence of both amplitude fluctuation and wavefront aberrations, when the ratio of receiving aperture diameter to coherent length is very large, Zuo et al. concluded that the Zernike mode is accurate [14,15]. With different ratio of receiving aperture diameter to coherent length, Liu and Huang et al. analyzed the ME and BER performance improvement of the coherent FSOC system through AO correction by numerical simulation using the experimental data from a 1.8 m telescope of 127 element AO system. The experimental results showed that the AO technique has great potential to improve the performance of the coherent FSOC, since AO is an effective method to compensate the atmospheric turbulence [16–19]. Until now most of the research works about the AO system are according to different ratio of receiving aperture diameter to coherent length. In our previous work, the performance analysis of a coherent FSOC system with AO unit based on different GF is given in [20]. But the analysis considering both the spatial characteristics and the temporal characteristics GF is very few.

On the basis of the above research achievements, the main contribution of this work is that we give the analysis on the relationship between ME and BER of coherent FSOC system according to coherent communication theory and the relationship between ME and far field beacon energy concentration under different atmospheric coherent length and GF. And we provide an AO experimental platform for the analysis of the coherent FSOC system based on an AO from both spatial and temporal characteristics of the atmospheric turbulence. ME, outage probability and BER of this coherent FSOC experiment platform with BPSK modulation is calculated to evaluate the ability of the AO system for suppressing the atmospheric turbulence.

2. System model

Our coherent FSOC system with an AO unit is illustrated in Fig. 1. In this system, Laser source emits laser beam modulated to be a laser carrier signal. Then it is transmitted through atmospheric link and arrives at receiving terminal. And its frequency is mixed with local oscillation (LO) signal to generate intermediate frequency signal. A demodulator and a digital signal processer complete the subsequent processing. Here, an AO unit is introduced to compensate the influence of atmospheric turbulence which disturbs both wavefront and amplitude of the laser carrier signal during signal transmission. The AO unit consists of three parts: wavefront sensor, wavefront corrector, and wavefront controller. The wavefront sensor can measure the wavefront aberrations from the atmospheric turbulence. The wavefront controller controls wavefront corrector according to the measured wavefront aberrations from the wavefront sensor. And the wavefront corrector performs wavefront correction [20].

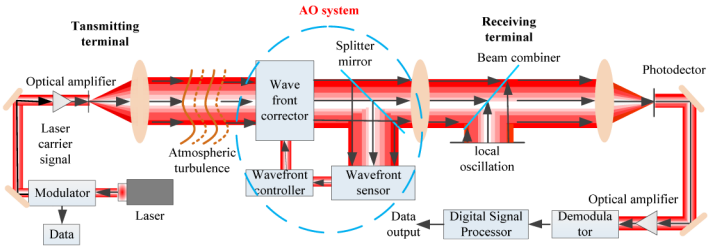

Fig. 1. Coherent FSOC system.

Optics EXPRESS

3. Theoretical basis

3.1 ME analysis

In assumption that the LO is a plane wave and the intensity of the received optical signal (OS) is uniform, the optical field distributions of the OS and LO can be expressed as [16]

$$E_S = A_S E^{i(2\pi f_S t + \varphi_S)} \tag{1}$$

$$E_{LO} = A_O E^{i(2\pi f_O t + \varphi_O)} \tag{2}$$

where A_S and A_O are the amplitudes of OS and LO respectively, f_S and f_O denote their frequencies,and φ_S and φ_O are the phases of OS and LO respectively.

According to the coherent detection theory, the total optical power at a photo-detector is given by

$$I = \int_S (E_{LO} + E_S)(E_{LO} + E_S)^* ds \tag{3}$$

Substituting Eqs. (1) and (2) into Eq. (3), we can obtain:

$$I = \int_S \left\{ A_O^2 + A_S^2 + 2A_O A_S \cos\left[2\pi(f_S - f_O) + \Delta\varphi\right] \right\} ds \tag{4}$$

where $\Delta\varphi = \varphi_S - \varphi_O$ denotes the phase difference between OS and LO, and S is the area of the receiver aperture. In Eq. (3), if $f_S = f_O$, we call it homodyne detection, if $f_S \neq f_O$, we call it heterodyne detection. Since the symbol transmission rate is generally less than 1 ns in the coherent FSOC system, GF is normally in the millisecond orders of magnitude, and the phase aberrations caused by atmospheric turbulence can be considered frozen during the detection time in every code. Thus $\Delta\varphi$ can be expressed by

$$\Delta\varphi = \varphi(r) + \varphi(t) \tag{5}$$

where $\varphi(r)$ is the time-independent phase aberrations from the atmospheric turbulence, and $\varphi(t)$ is the modulated phase of OS which is space coordinate-independent.

The ME of the homodyne detection is defined by [17]:

$$\eta = \frac{\left[\int_S \mathrm{A}_S \mathrm{A}_O \cos(\Delta\varphi) ds\right]^2}{\int_S \mathrm{A}_S^2 \, ds \int_S \mathrm{A}_O^2 \, ds} \tag{6}$$

According to Eq. (6), the ME is approximate to the Strehl ratio of the far-field images. The probability of the residual wavefront variance of an AO system in time domain provides more information on the AO system performance than the average index [21]. In this study, we adopt the probability pattern to analyze the relationship between the ME and average residual wavefront aberrations. Based on our previous work, considering the spatial and temporal characteristics, the average residual wavefront variance after AO correction can be expressed as [20,21]:

$$E(\sigma_\varphi^2) = \left[\alpha_F \left(\frac{d}{r_0}\right)^{5/3} + \kappa \left(\frac{f_G}{f_{3dB}}\right)^{5/3} \right] (rad) \tag{7}$$

According to Jian's work, Eq. (7) describes the average value of the residual wavefront variance. Thus, the relationship between the ME and the average residual wavefront variance can be expressed as [22,23]:

Optics EXPRESS

$$\eta \propto SR = \exp\left\{-\left[\alpha_F\left(\frac{d}{r_0}\right)^{5/3} + \kappa\left(\frac{f_G}{f_{3dB}}\right)^{5/3}\right]\right\} \tag{8}$$

where η is ME, SR is the Strehl ratio of the far-field images, α_F is the fitting error coefficient, f_G is GF, d is the equivalent distance between the actuators on the entrance pupil of the receiving antenna, r_0 is the atmospheric coherence length, f_{3dB} is the closed-loop control bandwidth (CLCB) of AO system, and κ is a constant. For the plane wave, κ=1.

3.2 BER analysis

In the coherent detection system, its BER is given by:

$$\mathrm{BER} = \frac{1}{2}\mathrm{erfc}\left(\frac{Q}{\sqrt{2}}\right) \tag{9}$$

where $\mathrm{erfc}(\cdot)$ is the complementary error function,and $Q = \sqrt{\mathrm{SNR}}$, where SNR is the signal to noise ratio of homodyne detection. For the synchronous BPSK received system, the optical power at the receiver is:

$$P_S = N_P h\nu B \tag{10}$$

The signal to noise ratio without atmospheric turbulence is:

$$\mathrm{SNR}_0 = \frac{2\delta P_S}{h\nu B} = 2\delta N_P \tag{11}$$

where SNR_0 is the signal to noise ratio without atmospheric turbulence, N_p is the number of photons received within single bit, and δ is quantum efficiency of the detector. The BER of the homodyne receiver is:

$$\mathrm{BER} = \frac{1}{2}\mathrm{erfc}\left(\sqrt{2\delta N_P \eta}\right) \tag{12}$$

3.3 Outage probability analysis

Outage probability is one of important performance criterion to evaluate digital wireless communication systems. The outage probability is defined as the probability that the instantaneous SNR falls below a specified threshold. For a given optical communication system, the outage probability can found by [24]:

$$P_{outage}(\gamma_T) = \Pr\{\gamma < \gamma_T\} = \int_0^{\gamma_T} f_\gamma(\gamma) d\gamma \tag{13}$$

where $\Pr\{\cdot\}$ denotes the probability of an event, γ_T is a predefined outage probability threshold, and $f_\gamma(\gamma)$ is the PDF of the instantaneous SNR. The instantaneous combiner SNR is independent of the local oscillator power for large local oscillator power, the local oscillator power does not affect coherent FSOC system performance [25]. Thus, γ is the SNR of received optical signal. According to Eq. (13), we will analyze the outage probability after AO correction by experimental data in this paper.

The performance of ME and BER is analyzed in detail under different GF in our previous work [20]. In this paper, we will concentrate ourselves to analyze the performance with different GF and r_0.

Optics EXPRESS

4. Numerical simulation

We assume the receiver is a homodyne detection scheme, and the intensity on the coherent plane is uniform. Considering horizontal-path transmission, the fluctuation of wind velocity is ignored. We select a wavelength of 1550 nm, the receiving antenna aperture is 1.2 m. In the previous work, we have given the relationship between the BER and the CLCB under different GF [20]. In this paper, we will give the relationship between the ME and the CLCB under different r_0 and GF. When GF is 90 Hz, the results of the ME under different r_0 are shown in Fig. 2.

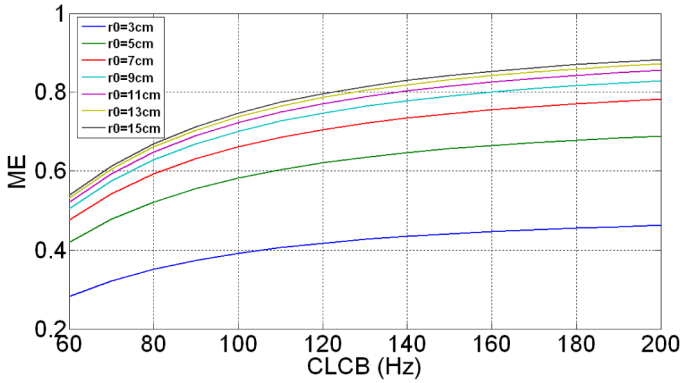

Fig. 2. ME versus CLCB when GF = 90 Hz.

As shown in Fig. 2, when the GF is 90 Hz, r_0 is 3 cm, the ME is about or below 0.45 with the CLCB is 60 Hz to 200 Hz, when CLCB is 60 Hz, ME is below 0.3. When r_0 is greater than 5 cm, the ME is above 0.4 with the CLCB is 60 Hz to 200 Hz. When the CLCB is more than 100 Hz, the ME is greater than 0.4 with different r_0. According to Eq. (12), when N_p = 10 and δ = 1, the relationship between the BER and the CLCB is shown as Fig. 3.

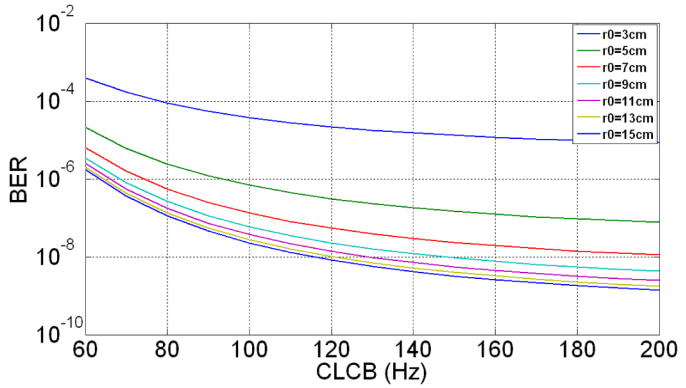

Fig. 3. BER versus CLCB when GF = 90 Hz.

As shown in Fig. 3, when the GF is 90 Hz, r_0 is 3 cm, the BER is above 10^{-5} with the CLCB is 60 Hz to 200 Hz. When r_0 is 15 cm, the BER is below 10^{-8} when CLCB is more than 120 Hz.

5. Analysis of experiment results

An AO experiment system is setup with a double stage fast-steering-mirror (FSM) and a 97-element continuous surface deformable mirror to analyze the performance improvement under different r_0 and GF. This experiment system is designed to match a 1.2 m aperture

Optics EXPRESS

telescope. The wavelength of the laser is 532 nm. The Shack-Hartmann (S-H) wavefront sensor operates at 550 nm, and we transform the residual aberrations data at 1550 nm consistent with the communication wavelength. The schematic diagram of the system is described in Fig. 4 [20].

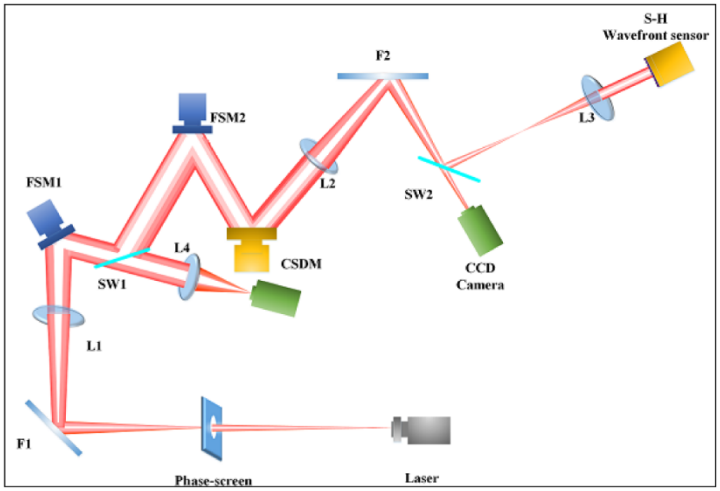

Fig. 4. Structure of our experiment system.

As shown in Fig. 4, double FSMs, S-H wavefront sensor, and a 97-element continuous surface deformable mirror are introduced in our experiment system in order to correct the aberrations. The focal lengths of L1 and L3 are 400 mm and 3000 mm respectively, and the apertures of L1 and L3 are 76 mm. The focal lengths of L2 and L4 are 3000 mm and 300 mm respectively, and the apertures of L2 and L4 are 80 mm. The high speed and large stroke FSM made in the PI Corporation are separately chosen in the double stage FSM unit. The first stage FSM uses a high speed short wave infrared camera as the measuring camera, the maximum frame frequency can reach 400 Hz, and the pixel size is 20 μm. The second stage FSM is driven according to the tilt value measured by the S-H wavefront sensor with high speed camera at 500 Hz frame frequency. A continuous surface deformable mirror is used to correct high-order aberrations, and the stroke of actuators is 5 μm. The number of the effective sub-apertures is 97. The aperture and focal length of micro-lens are 200 μm and 7 mm respectively [20].

To simulate different atmospheric turbulence, the phase screen from Lexitek company is used and it satisfies the Kolmogrov turbulence theory. We can change r_0 through adjusting the clear aperture given as:

$$\frac{D}{r_0} = \frac{D_t}{r_{0t}} \tag{14}$$

where D is the receiving antenna aperture, r_{0t} is the coherent length of phase screen, D_t is the aperture size of the phase screen. And we can adjust GF by controlling the rotate speed of phase screen. The photo of our designed experiment system is shown in Fig. 5.

Optics EXPRESS

Fig. 5. Photo of our experiment system.

In this section, we will analyze ME, outage probability and BER of the given coherent FSOC system in different r_0 and GF under certain SNR. The ME is approximate to the Strehl ratio of far field images. And it is defined by the ratio of far field encircled energy to the diffraction limited encircled energy.

In our experiments, the variation of r_0 and GF are simulated by changing the location and rotate speed of the phase screen, and their influence on the coherent FSOC system based on AO from both spatial and temporal characteristics of atmospheric turbulence is discussed in detail as follows.

In our experiments, the CLCB of this system is 60 Hz. When r_0 is 5 cm, under different GF, the far field images are shown in Fig. 6.

Optics EXPRESS

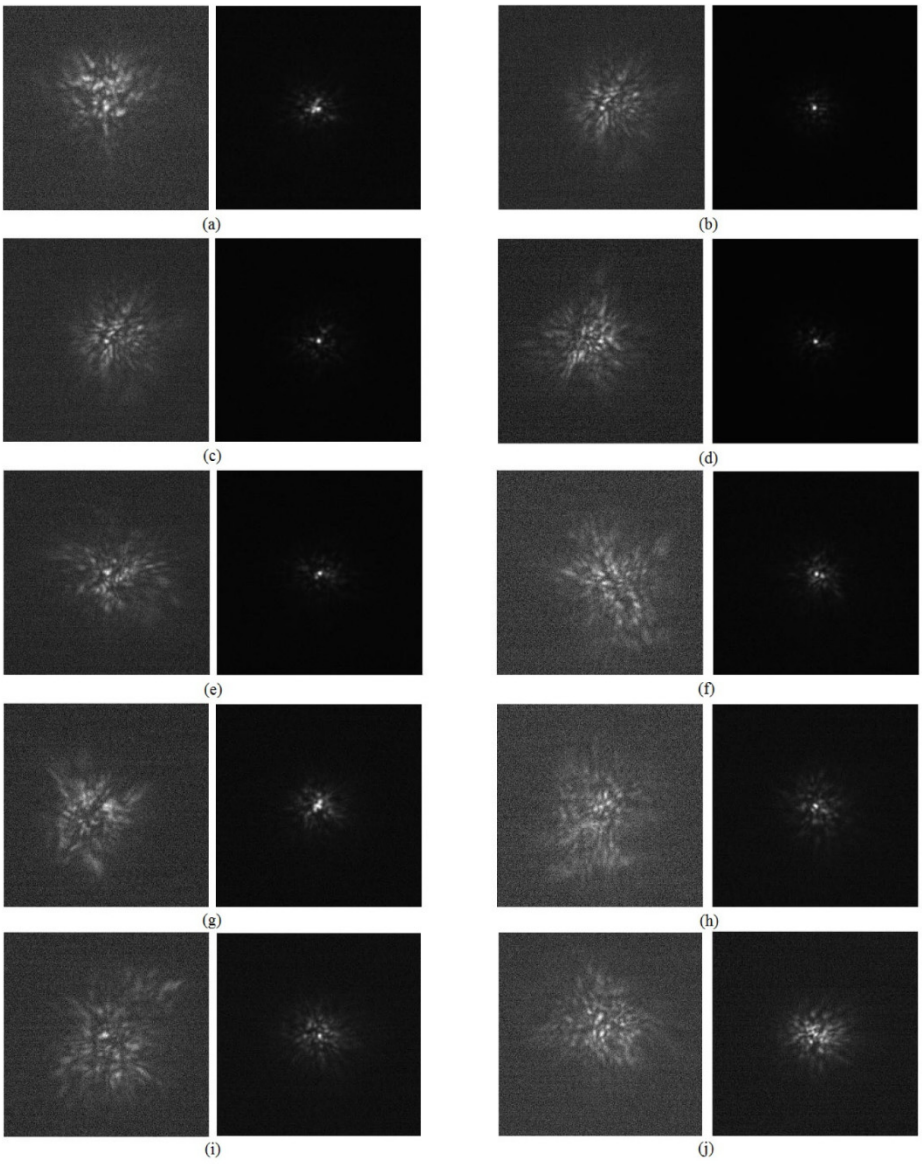

Fig. 6. Far field images before and after correction (r_0 = 5 cm) with different GF, where are the images when GF = 10 Hz to GF = 100 Hz from (a) to (j).

As shown in Fig. 6, the impact of temporal characteristics on the laser energy concentration degree is obvious. With the increase of GF, the energy concentration degree of the far filed laser images decrease gradually. This implies that the temporal characteristics have influence on the corrected results of the AO system, which is limited by the closed-loop bandwidth of the control system. The performance after the closed-loop correction is better when GF is less than 50 Hz.

In order to analyze the impact of the temporal characteristics on the correction ability of the AO system, we adjust GF to 60 Hz. With different r_0, the far field laser images after correction by the AO system are shown in Fig. 7.

Optics EXPRESS

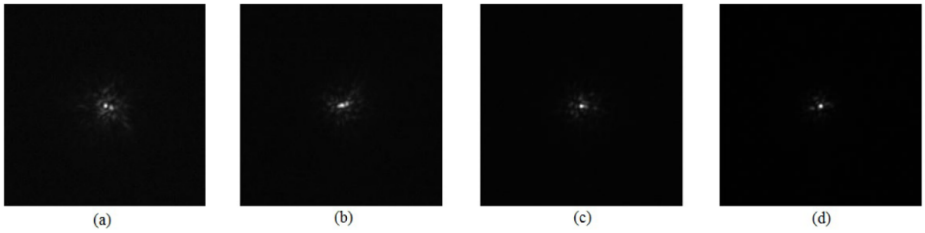

Fig. 7. Far field images before and after correction (GF = 60 Hz) with different r_0, where (a) is r_0 = 5 cm, (b) is r_0 = 7 cm, (c) is r_0 = 9 cm and (d) is r_0 = 11 cm.

From Fig. 7, we find that the larger r_0 is, the stronger correction ability of the AO close-loop control unit has and the higher beacon energy concentration level will be achieved. Based on the coherent FSOC theory, the far field beacon energy concentration level is represented by the encircled Strehl ratio. According to the relationship between ME and the Strehl ratio of the far field images, when r_0 is 5 cm, the ME under different GF during AO correction is shown in Fig. 8.

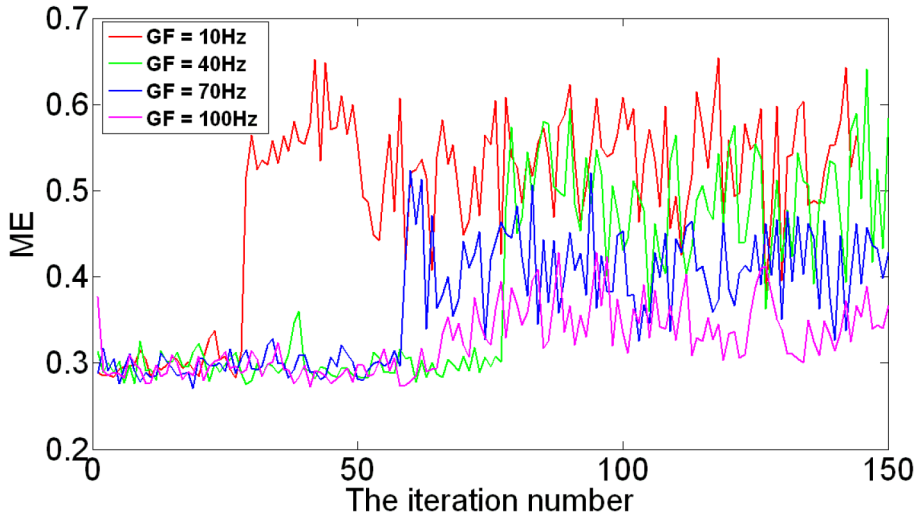

Fig. 8. ME versus iteration number when r_0 = 5 cm with different GF.

In Fig. 8, when r_0 = 5 cm, the system ME is about 0.3 under different GF without AO correction. But we can find that after correction, the ME can reach 0.5 when GF is 10 Hz and 40 Hz respectively. Because of the limitation of the close-loop control bandwidth, when GF is larger than 70 Hz, the ME is only about 0.4 after correction.

As shown in Fig. 8, after correction, when GF is 10 Hz, the mean of ME is 0.5309 and the variance is 0.0034. When GF is 40 Hz, the mean of ME is 0.4878 and the variance is 0.003. When GF is 70 Hz, the mean of ME is 0.4144 and the variance is 0.0019. And when GF is 100 Hz, the mean of ME is 0.3498 and the variance is 0.0011. The results are consistent those shown in Fig. 10 of Ref [23].

In other perspective, we also give the relationship between the system ME and iteration number after correction, when GF is 60 Hz with different r_0 in Fig. 9. According to Fig. 9, when r_0 is 5 cm, the ME after correction is only about 0.45, and when r_0 is larger than 7 cm, the ME is above 0.5. We can also observe that the system ME after the close-loop correction by the AO unit increases obviously with the growth of r_0.

Optics EXPRESS

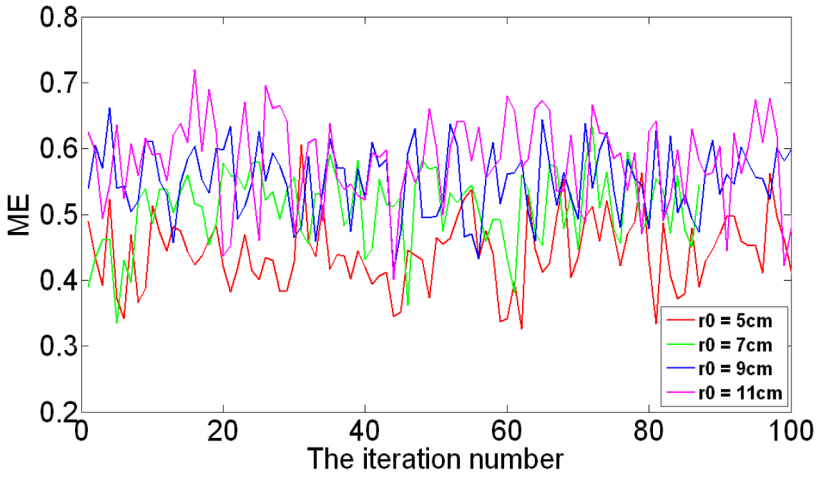

Fig. 9. ME versus iteration number when GF = 60 Hz with different r_0.

As shown in Fig. 9, when r_0 is 5 cm, the mean of ME is 0.4412 and the variance is 0.0032. When r_0 is 7 cm, the mean of ME is 0.5099 and the variance is 0.0026. When r_0 is 9 cm, the mean of ME is 0.5503 and the variance is 0.0028. And when r_0 is 11 cm, the mean of ME is 0.5814 and the variance is 0.003. The results are basically in concordance with those provided in Fig. 10 of Ref [23].

Assuming the quantum efficiency is 1, and N_p = 10, in the case of r_0 = 5 cm, according to Eq. (12), we present the system BER before and after AO correction in Table 1. From Table 1, we can see that when GF is 10 Hz and 40 Hz, the BER decreases from 10^{-3} to below or nearly 10^{-5}. However, when GF is 70 Hz and 100 Hz, the BER is larger than 10^{-5} due to the limitation of the close-loop control bandwidth.

Table 1. BER before and after when r_0 = 5 cm with different GF.

GF	Mean of BER before correction	Mean of BER after correction
10 Hz	1.3×10^{-3}	2.1×10^{-6}
40 Hz	2.6×10^{-3}	1.1×10^{-5}
70 Hz	5.7×10^{-3}	3.5×10^{-5}
100 Hz	8.4×10^{-3}	1.5×10^{-4}

Then we adjust r_0 by changing the locations of the phase screen, when GF is 60Hz, to obtain the BER before and after correction under different r_0 which is shown in Table 2. From Table 2, when GF is 60 Hz, we find that the smaller r_0 is, the stronger influence on the correction of the AO system is. When r_0 is larger than 7 cm, the BER after corrections is below 10^{-6}. And when r_0 is 5 cm, the BER after close-loop corrections only reach to around 10^{-5}.

Table 2. BER after correction when GF = 60 Hz with different r_0.

r_0	Mean of BER after correction
5 cm	1.1×10^{-5}
7 cm	2.3×10^{-6}
9 cm	1.6×10^{-6}
11 cm	6.7×10^{-7}

Then, we summarize the experimental results with different r_0 and GF in Table 3, including the ME and BER after AO correction. According to Table 3, when r_0 is larger than 7 cm, the mean of ME is more than 0.5 under different GF. When r_0 is 11 cm, the ME can reach nearly 0.6 and the corresponding BER is about 10^{-6}. For the same GF, if r_0 reduces from 11 cm to 5 cm, the BER will increase one or two orders of magnitude. Similarly, for the

Optics EXPRESS

same r_0, when GF increases from 10 Hz to 100 Hz, the BER will increases two or three orders of magnitude. From the analysis of these simulation results, we can conclude that the influence of the temporal characteristics is slightly stronger than that of the spatial characteristics.

Table 3. Experimental results under different GF and r_0.

r_0	GF	Mean of ME	Mean of BER	r_0	GF	Mean of ME	Mean of BER
5 cm	10 Hz	0.5309	4.33×10^{-6}	7 cm	10 Hz	0.6445	3.28×10^{-7}
	20 Hz	0.5261	4.80×10^{-6}		20 Hz	0.6231	4.47×10^{-7}
	30 Hz	0.5086	5.65×10^{-6}		30 Hz	0.5912	8.41×10^{-7}
	40 Hz	0.4878	9.58×10^{-6}		40 Hz	0.5693	1.86×10^{-6}
	50 Hz	0.4700	1.34×10^{-5}		50 Hz	0.5392	3.08×10^{-6}
	60 Hz	0.4412	2.41×10^{-5}		60 Hz	0.5099	7.58×10^{-6}
	70 Hz	0.4144	3.66×10^{-5}		70 Hz	0.4677	1.31×10^{-5}
	80 Hz	0.3866	6.35×10^{-5}		80 Hz	0.4480	1.80×10^{-5}
	90 Hz	0.3652	8.02×10^{-5}		90 Hz	0.4115	3.79×10^{-5}
	100 Hz	0.3498	1.11×10^{-4}		100 Hz	0.3937	4.84×10^{-5}
Mean		0.4481	3.53×10^{-5}	Mean		0.5198	1.32×10^{-5}
r_0	GF	Mean of ME	Mean of BER	r_0	GF	Mean of ME	Mean of BER
9 cm	10 Hz	0.6646	1.86×10^{-7}	11 cm	10 Hz	0.7027	7.11×10^{-8}
	20 Hz	0.6530	1.88×10^{-7}		20 Hz	0.7033	7.27×10^{-8}
	30 Hz	0.6449	3.03×10^{-7}		30 Hz	0.6832	1.26×10^{-7}
	40 Hz	0.6106	6.77×10^{-7}		40 Hz	0.6463	4.53×10^{-7}
	50 Hz	0.5901	8.53×10^{-7}		50 Hz	0.6221	5.43×10^{-7}
	60 Hz	0.5503	2.52×10^{-6}		60 Hz	0.5814	2.08×10^{-6}
	70 Hz	0.5092	6.27×10^{-6}		70 Hz	0.5380	4.58×10^{-6}
	80 Hz	0.4730	1.37×10^{-5}		80 Hz	0.5077	9.34×10^{-6}
	90 Hz	0.4469	1.96×10^{-5}		90 Hz	0.4954	1.01×10^{-5}
	100 Hz	0.4217	3.32×10^{-5}		100 Hz	0.4799	1.18×10^{-5}
Mean		0.5564	7.75×10^{-6}	Mean		0.5960	3.91×10^{-6}

In this paper, for the coherent FSOC system with BPSK modulation, we assume $N_p = 20$ and $r_0 = 5$ cm, then we give the BER before and after close-loop correction of the AO unit under different GF in Table 4. As shown in Table 4, the BER after the correction can be below 10^{-7}. Interestingly, considering the CLCB is nearly 60 Hz, when GF is more than 70 Hz, the BER is nearly around 10^{-8} after correction. When GF is 40 Hz, the BER can be about 10^{-9} after correction. And when GF is 10 Hz, the BER can reach below 10^{-9} after correction.

Table 4. BER before and after correction when $r_0 = 5$ cm and $N_p = 20$ with different GF.

GF	Mean of BER before correction	Mean of BER after correction
10 Hz	1.1×10^{-6}	1.7×10^{-10}
40 Hz	3.5×10^{-6}	2.2×10^{-9}
70 Hz	5.5×10^{-6}	1.9×10^{-8}
100 Hz	7.9×10^{-6}	1.4×10^{-7}

In the case of $N_p = 20$ and GF is 60 Hz, the BER after close-loop correction under different r_0 is shown in Table 5. From Table 5, for different r_0, the system BER can reduce to

Optics EXPRESS

10^{-8}. And when r_0 is larger than 5 cm, the BER can attain below 10^{-9}. When r_0 = 11 cm, the BER of coherent FSOC system can even reach 10^{-11} after correction.

Table 5. BER after correction when GF = 60 Hz and N_p = 10 with different r_0.

r_0	Mean of BER after correction
5 cm	8.9×10^{-9}
7 cm	1.4×10^{-10}
9 cm	8.5×10^{-11}
11 cm	5.5×10^{-12}

Finally, we analyze the outage probability after AO correction with different GF when r_0 is 5 cm. Here, we select γ_T = 10 dB. The outage probability after correction versus GF is shown in Fig. 10.

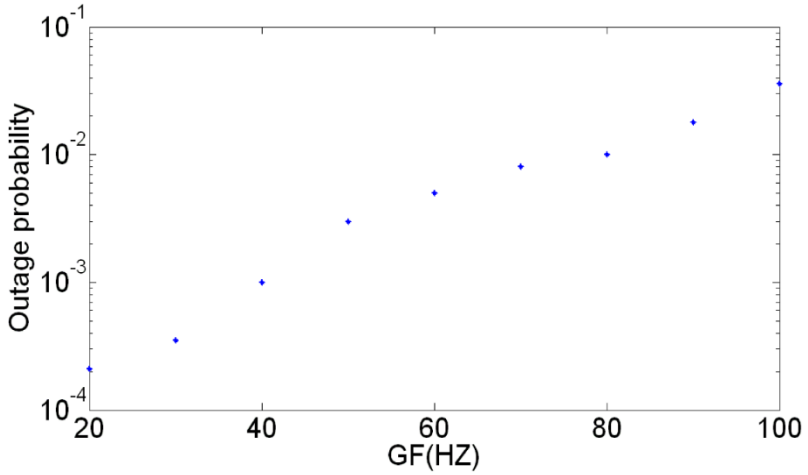

Fig. 10. Outage probability after AO correction versus GF when r_0 is 5 cm.

As shown in Fig. 10, after AO correction, when GF is below 50 Hz, the outage probability is below or about 10^{-3}. When GF is above 80 Hz, the outage probability is above or about 10^{-2}.

From the analysis above, it is clearly known that the negative influence of atmospheric turbulence on ME, outage probability and BER of coherent FSOC system can be suppressed by AO unit. This means that the AO unit can play important and effective role for the communication in different atmospheric space and temporal characteristics. Comparing Table 4 with Table 5, if the receiving aperture and the number of sub-apertures are given, we find again that the influence of the atmospheric temporal characteristics is slightly stronger than that of the spatial characteristics.

5. Discussion and conclusion

In this paper, based-on our previous work and the AO experimental platform, we present the analysis of the impact of atmospheric temporal characteristics and spatial characteristics for the performance of the AO unit for the given coherent FSOC system. Under different atmospheric coherent length and GF, the system ME, outage probability and BER before and after correction are given with BPSK modulation.

The experimental results are shown in Table 3, including the ME and BER after AO correction, under different r_0 and GF. The results show that the BER can increase one or two orders of magnitude along with the reduction of r_0. And for the same r_0, the BER increase two or three orders of magnitude with the increase of GF. In addition, the outage probability after AO correction is provided through experimental data. The results show that the outage

Optics EXPRESS

probability increases along with GF. The results show that when the receiving aperture and the number of sub-apertures are given, there is stronger influence from the atmospheric temporal characteristics compared with that from the spatial characteristics.

Thus, the performance will be improved further by enlarging the CLCB through increasing sampling and the resonant frequency. An experimental coherent FSOC system with an AO unit will be building, and then the ME, outage probability and BER will be measuring by special instruments in the future work.

Acknowledgments

The authors acknowledge helpful suggestions from the reviewers and help from the editors. This work was supported by National Natural Science Foundation of China (No. 61601195 and No. 61605199) and China Postdoctoral Science Foundation (2016M590255).